APPENDIX F: Hydroclimatic reconstructions in the Lower Basin: Winter precipitation reconstruction of the Bill Williams watershed

by Kiyomi Morino and David Meko,
Laboratory of Tree-Ring Research, The University of Arizona

Table of Contents

F.1 Introduction

The completion of Alamo Dam in 1968 greatly altered the natural streamflow regime of The Bill Williams River. Daily natural flows above Alamo Lake were, however, estimated for the purposes of developing water resource management plans by the Army Corps of Engineers. These data were used to assess the potential for developing a streamflow reconstruction. Preliminary streamflow reconstruction models showed a poor fit to the data, likely due to the combination of a highly flashy streamflow regime and insufficient number of tree-ring sites in and near the watershed. As a result, the potential for a precipitation reconstruction was explored. Exploratory comparisons between individual candidate sites and both Water Year and winter, October through April, precipitation indicated relatively high correlations with a stronger association between tree-ring indices and winter precipitation. This hydroclimatic variable was subsequently targeted for reconstruction.

F.2 Study Basin

Below Lake Mead, the Bill Williams River is the second largest tributary to the Colorado after the Gila River. It is formed at the confluence of the Big Sandy and Santa Maria Rivers and drains an area more than 13,000 km^2 (3.2 million acres) of rugged and physiographically diverse terrain. Elevations within the watershed range from 137 m (449 ft) at its confluence with the Colorado River at Lake Havasu to 2566 m (8417 ft) at Hualapai Peak in the Big Sandy sub-basin (Shafroth and Beauchamps 2006). The Bill Williams River watershed contains four sub-basins: Big Sandy (HUC is 15030201); Burro (HUC is 15030202); Santa Maria (HUC is 15020303); and Bill Williams (HUC is 15020304).

F.3 Data

F.3.1 Precipitation Data

Precipitation data were derived from PRISM (Precipitation-elevation Regressions on Independent Slopes Model) data (Gibson et. al 2002). Monthly PRISM data, 1900-2010, for the continental US were downloaded from the PRISM site (http://prism.oregonstate.edu/products/). Data pertaining to the Bill Williams River basin were "clipped" from the larger dataset using a script written in MatLab ™. Average precipitation depth in mm over the entire basin was computed. Precipitation is strongly bimodal with a large pulse of moisture occurring in August (Figure F-1).

F.3.2 Tree-Ring Data.

Tree-ring data for this reconstruction consisted of measured ring-widths. These were obtained from the International Tree-Ring Data Bank (ITRDB) (http://www.ncdc.noaa.gov/paleo/treering.html) and from new sites collected not yet submitted to the ITRDB (Table F-1). Although the reconstruction generated in this study made use of 8 tree-ring chronologies, the starting tree-ring data before screening consisted of ring widths from 14 sites in or near the basin. Sites were selected with the

criteria that the species be moisture-sensitive and the data cover at least the period 1750-1945. The 1750 cutoff ensured that at least two centuries of reconstructed streamflow data could be later analyzed for patterns of temporal variability; the 1945 cutoff ensured a reasonably long period (45 years) for calibration of precipitation with tree rings in the reconstruction model.

See *Hydroclimatic Reconstructions in the Lower Basin of the Colorado River, METHODS* for details regarding tree-ring data standardization.

Following chronology development, both water year and winter, October through April, precipitation were compared to tree-ring data using simple correlation analysis. Winter precipitation showed a stronger association with the tree-ring data and was targeted for reconstruction.

F.4 Methods

F.4.2 Reconstruction Model

See *Hydroclimatic Reconstructions in the Lower Basin of the Colorado River, METHODS* for details regarding methods employed in single-site reconstructions.

F.5 Results and Discussion

F.5.1 Reconstruction modeling

Tree-Ring Chronology Development

The reduced set of 11 tree-ring chronologies passing the screening for sample depth and correlation with flow are listed in Table F-1. Their site locations are marked by shaded triangles on the map in Figure F-2. The common period is 1699-1947, though some extend to earlier and later years. Exploratory correlation analysis pointed to 1600 as a feasible start year for reconstruction. All chronologies were therefore truncated to start in either 1600 or the first year with adequate subsample signal strength (SSS>0.85). Descriptive statistics showed that the chronologies have near-zero autocorrelation and negative skew (Table F-2). Skew is significantly (p<0.01) negative for two chronologies. The near-zero autocorrelation is expected, as these are residual chronologies (Cook et al. 1990b).

Single-Site Reconstruction

The SSR models explain 19-54 percent of the variance of precipitation in the calibration period, which ranges in length from 64 to 109 years for the 11 sites (Table F-3). Calibration periods start with 1901 but end in different years (1965 to 2010) depending on either the collection date of the chronology or the last year of precipitation data, 2010. All models have some skill of verification, as indicated by an RE-statistic above zero.

The final selected smoothing parameter, α , for the SSR models ranges from 0.35 to 0.90. The variation in selected α reflects differences in curvature of the statistical relationship between precipitation and tree-ring index. Higher values indicate a more linear relationship.

Recalibration and Reconstruction
Summary statistics of the loess models used to recalibrate the scores of PC#1 of the SSRs into final estimates of winter precipitation are listed in Table F-4. The percentage of precipitation variance explained by the models ranges from 50 percent for Models A and C to 58 percent for Model B. All three models have positive skill, reflected by positive RE statistics for cross-validation, and the root-mean-square error increases only slightly (<6 percent) from the calibration to the validation data. The loadings for PC#1 of each of the models are shown in Figure F-3. Few sites are located within the watershed. One of the newly collected sites, however, Antelope Wash, figures strongly in Models B and C.

Uncertainty
The validation statistics mirror the calibration R^2 in supporting the superior accuracy of Model B over the other two models (Table F-4). Statistics for Model B are most relevant, as that model supplies most of the reconstructed precipitation values. The RMSE of cross-validation of Model B is 50.2 mm (2.0 in), which is about two-thirds of the standard deviation of winter precipitation for the 1901-1986 calibration period of the model.

F.5.2 Reconstructed precipitation

Reconstructed winter precipitation, 1603-2008, is plotted in Figure F-5A along with a baseline at the long-term median of 168 mm (6.6 in) to facilitate identification of wet years and dry years. Reconstructed precipitation has a mean of 166 mm (6.5 in), is negatively skewed (skew =-0.22, p>0.05), not significantly autocorrelated (r_1=-0.027, p>0.05), and comparable to PRISM data, whose 1901-2010 mean is 169 mm (6.7 in).

The late 1800s and mid-1900s stand out in the long-term plot of reconstructed winter precipitation as the driest periods on record (Figure F-5B). For these two periods, the frequency of years below the median in a 30-year sliding window peaks at about two-thirds of the years "dry". In contrast, the early 1600s and mid 1800s stand out as the wettest periods in the reconstructed records, registering about two-thirds of the years as "wet."

F.6 Conclusions

Insufficient skill in reconstructing Bill Williams streamflow, likely due to a combination of flashy flow regime and low tree-ring site density in and around the Bill Williams watershed, led to the undertaking of a precipitation reconstruction. Winter precipitation was reconstructed with reasonable skill, explaining up to 58 percent of the variance in PRISM-derived winter precipitation estimates for the entire basin. Notable dry periods in the basin are relatively recent, occurring in the late 1800s, more recently, in the mid-1900s. The reconstruction of winter precipitation, while fairly skillful, would likely be improved with increased sampling of tree-rings within and around the Bill Williams watershed.

TABLES

Table 1. List of site chronologies.

N[1]	Site[2]	Species[3]	Location[4] Lat	Lon	El(m)	Period[5]
1	Antelope Wash	PIPO	35.1	-113.9	1893	1598-2008
2	Mayer	PIPO	34.4	-112.3	1951	1620-1965
3	Granite Mountain	PIPO	34.6	-112.5	2134	1695-1947
4	Dry Creek	PIED	34.9	-111.8	1377	1630-1986
5	Ord Mountain	PIPO	33.5	-111.2	2133	1570-1987
6	Rocky Gulch	PIPO	34.4	-111.3	1965	1670-1986
7	Slate Mountain	PIPO	35.5	-111.8	2194	1590-1986
8	Red Butte	PIED	35.8	-112.1	1920	1415-2005
9	Six Trail	PIPO	34.8	-112.9	1800	1682-2011
10	Ten Trail	PIPO	34.8	-112.9	1786	1699-2011
11	Walnut Canyon	PIPO	35.2	-111.5	1995	1528-2010

1 Site number
2 Site name
3 Species code: PIPO is *Pinus ponderosa*; PIED is *Pinus edulis*
4 Latitude and longitude in decimal degrees, elevation in m above sea level
5 Start and end year of chronology, after trimming as described in text

Table 2. Chronology basic statistics.

						Replication and Common Signal[4]		
N	Length[1]	Mean	Stdev	Skew[2]	r(1)[3]	#Cores	SSS	EPS
1	394(167)	0.998	0.253	-0.41**	-0.04	5-40	0.87	0.84-0.97
2	217(156)	1.007	0.263	-0.30	0.08	4- 6	0.89	0.66-0.75
3	217(156)	1.007	0.263	-0.30	0.08	4- 6	0.89	0.66-0.75
4	335(224)	1.000	0.252	0.00	-0.02	4-25	0.89	0.86-0.97
5	388(175)	1.000	0.202	-0.27*	-0.00	5-19	0.89	0.83-0.94
6	286(215)	0.995	0.178	-0.17	-0.03	5-25	0.87	0.83-0.96
7	329(158)	0.997	0.227	-0.18	0.02	4-37	0.88	0.86-0.98
8	406(162)	1.002	0.218	-0.14	-0.04	13-92	0.95	0.94-0.99
9	241(168)	0.998	0.268	-0.27	0.01	4-28	0.87	0.84-0.97
10	299(159)	1.001	0.175	-0.27	-0.01	5-35	0.86	0.83-0.97
11	408(156)	1.001	0.205	-0.40**	-0.01	6-86	0.88	0.87-0.99

1 Length of site chronology, with minimum segment length in parentheses
2 Skewness (*,** denote significance at 0.05, 0.01 level)
3 First-order autocorrelation (*,** denote r(1) significantly different from zero at 0.05, 0.01 level)
4 Range in number of cores, minimum value of subsample signal strength, and range in expressed population signal

Table 3. Summary of single-site loess models.

	Calibration[2]			Validation[3]		
N[1]	Period	α	V	RMSE	RE	RMSE	Group[4]
1	1901-2008	0.35	0.48	900.1	0.44	945.2	BC
2	1901-1965	0.50	0.40	825.2	0.32	889.0	
3	1901-1965	0.50	0.40	825.2	0.32	889.0	
4	1901-1986	0.45	0.54	787.8	0.49	838.1	B
5	1901-1987	0.90	0.29	971.7	0.25	1014.3	AB
6	1901-1986	0.60	0.24	1014.4	0.17	1070.5	
7	1901-1986	0.75	0.21	1033.6	0.16	1077.5	B
8	1901-2005	0.40	0.49	895.8	0.43	948.4	AB
9	1901-2010	0.80	0.43	935.6	0.41	960.4	C
10	1901-2010	0.65	0.19	1114.3	0.15	1152.5	C
11	1901-2010	0.50	0.24	1080.1	0.19	1123.9	ABC

1 Site number, as in Table 1
2 Calibration statistics: N=period for estimation of loess curve, α=loess smoothing parameter,V=variance-explained decimal fraction, RMSE=root-mean-square error of calibration
3 Validation statistics from leave-1-out cross-validation: RE=reduction of error statistic, RMSE=root-mean-square error
4 Subperiod reconstruction groups, see Table 4

Table 4. Summary of sub-period reconstruction models.

N[1]	Period[2]	p[3]	Calibration[4] α	Calibration[4] V	Calibration[4] RMSE	Validation[5] RE	Validation[5] RMSE
A	1603-1987	3	0.50	0.50	51.4	0.46	54.2
B	1658-1986	6	0.40	0.58	47.3	0.54	50.2
C	1771-2008	4	0.60	0.50	55.7	0.48	57.5

1 Sub-period model name
2 Starting and ending years of sub-period
3 Number of chronologies
4 Calibration statistics: α=loess smoothing parameter, V=variance-explained decimal fraction, RMSE=root-mean-square error of calibration
5 Validation statistics from leave-1-out cross-validation: RE=reduction of error statistic, RMSE=root-mean-square error

FIGURES

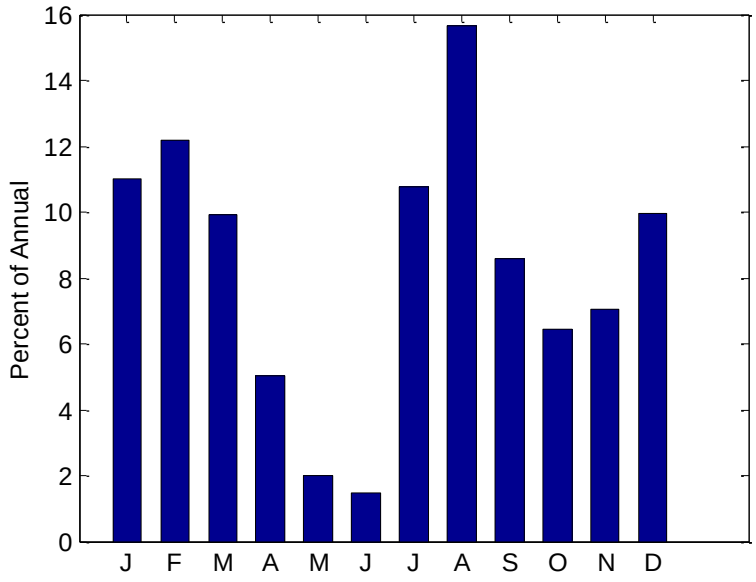

Figure 1. Monthly basin precipitation.

Bar charts summarizing annual distribution of monthly basin precipitation, 1900-2010. Data from PRISM.

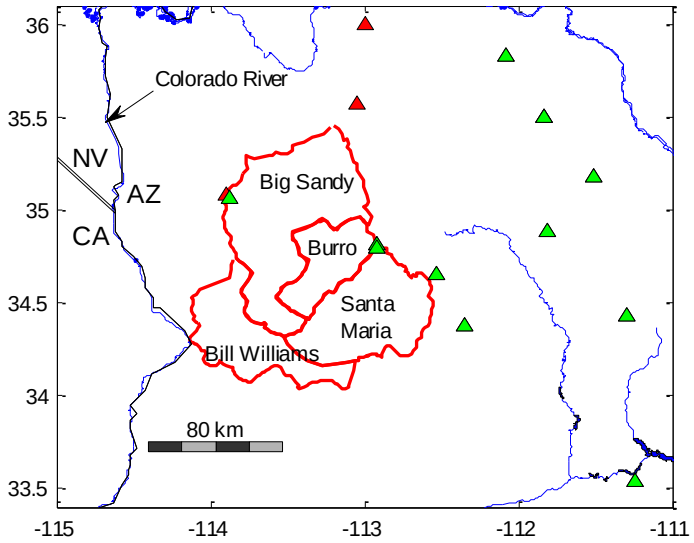

Figure 2. Site map.

Map showing Bill Williams sub-watersheds and tree-ring site locations. Tree-ring sites that passed screenings for sample depth and correlation with precipitation are denoted by green triangles. Tree-ring sites that did not pass screenings are denoted by red triangles.

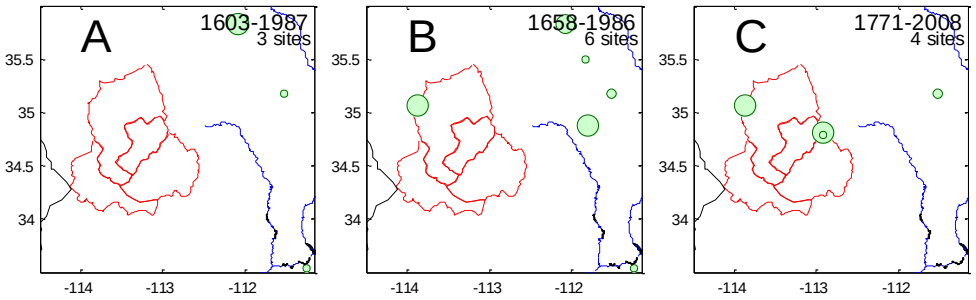

Figure 3. PC loadings.

Tree-ring site locations for sub-period reconstruction models. Models A, B and C coded as in Tables 4. Symbol sizes reflect magnitude of loadings of sites on PC#1 of SSRs.

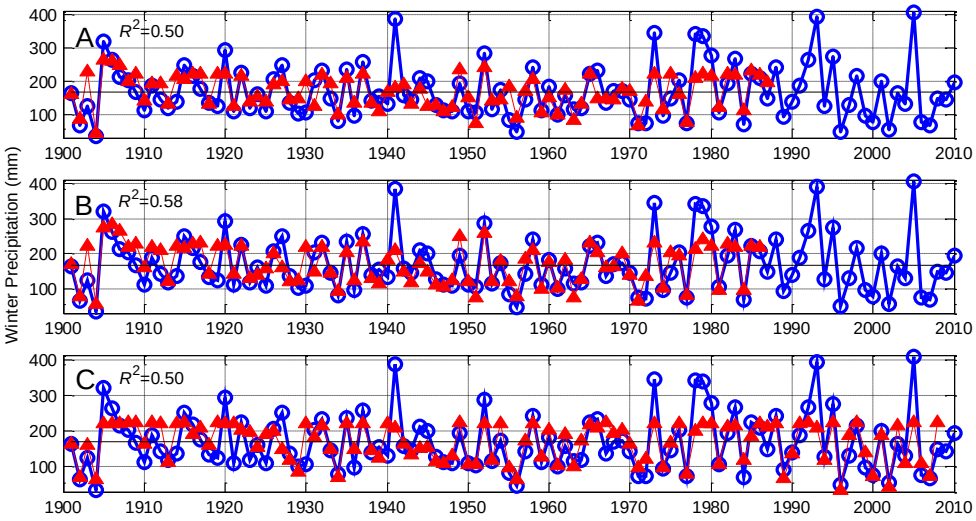

Figure 4. Agreement of observed and reconstructed precipitation.

Agreement of observed and reconstructed precipitation for three sub-period models (as coded in Table 4). Annotated at upper left is the variance explained by the model. Horizontal line is the observed mean precipitation for the period, 1900-2010.

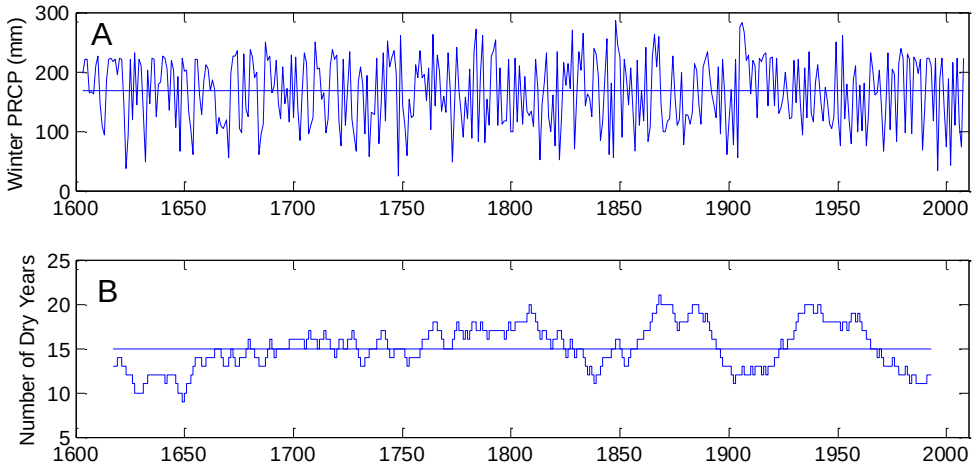

Figure 5. Time plots of reconstructed winter precipitation.

Time plots of reconstruction and dry-year frequency. (A) Reconstructed precipitation, 1603-2008, and dry year threshold (horizontal line) at median. (B) Frequency of dry years in centered 30-year moving window. Horizontal line in (B) is expected number of dry years in 30-year window.